Journal of the Mechanics and Physics of Solids 126 (2019) 87–100

Contents lists available at ScienceDirect

Journal of the Mechanics and Physics of Solids

journal homepage: www.elsevier.com/locate/jmps

Experimental and finite element analyses of contact behaviors between non-transparent rough surfaces☆

Feikai Zhang, Jianhua Liu, Xiaoyu Ding*, Runliang Wang

Beijing Institute of Technology, School of Mechanical Engineering, 5 South Zhongguancun Street, Haidian District, Beijing 100081, China

ARTICLE INFO

Article history:
Received 15 September 2018
Revised 10 December 2018
Accepted 2 February 2019
Available online 6 February 2019

Keywords:
3D contact analyses
Contact mechanics
Finite element method
Real contact area
X-ray computed tomography

ABSTRACT

The real contact area and separation between rough surfaces are significant parameters in sealing, tribology, and lubrication. However, it is challenging to experimentally observe the contact behaviors between rough surfaces because the materials of rough surfaces are usually non-transparent and not accessible for direct visual observation. In this study, X-ray computed tomography was used to directly measure the contact behaviors between rough surfaces. The real contact area and three-dimensional surface separation of contact pairs made of aluminum and polycarbonate were experimentally measured. In addition, finite element models were developed to simulate the contact behaviors of the same contact pairs. The results obtained from the finite element analyses and the experiments were compared. The simulation results were in good agreement with the experimental observations when the material properties of the rough surfaces were consistent.

1. Introduction

Contact mechanics plays important roles in several fields including tribology, lubrication, and sealing (Yastrebov et al., 2015). The area of the contact zone, which is called the real contact area, and the surface separation are significant contact mechanics parameters requiring prediction. Extensive research has been published on how the real contact area and surface separation change with squeeze load and surface material.

Pioneering work on contact mechanics was first conducted (Müser et al., 2017) by Greenwood and Williamson (1966), and their asperity model is called the GW model. This model assumes that a rough surface is covered with asperities of random heights and spherical shapes, and the contact behavior of each asperity is Hertzian (Hertz, 1881). Subsequent asperity models take the effects of plastic deformation (Chang et al., 1987; Zhao et al., 2000), asperity interaction (Zhao and Chang, 2001; Ciavarella et al., 2006; Ciavarella et al., 2008; Paggi and Ciavarella, 2010; Afferrante et al., 2012), asperity coalescence (Afferrante et al., 2012), and stick-slip behavior (Wang et al., 2017) into consideration. All of these models are quite accurate under small squeeze loads; however, their error rates dramatically increase with increasing load (Yastrebov et al., 2015). Persson (2001) pioneered another class of analytical models, introducing a diffusion equation that describes how the probability density of the contact pressure varies with the surface roughness. This equation was extended to finite pressures

☆ The English in this document has been checked by at least two professional editors, both native speakers of English. For a certificate, please see: http://www.textcheck.com/certificate/JNIOLs.

* Corresponding author.
E-mail addresses: zhangfkbit@163.com (F. Zhang), jeffliu@bit.edu.cn (J. Liu), xiaoyu.ding@bit.edu.cn (X. Ding), runliang_wang@163.com (R. Wang).

https://doi.org/10.1016/j.jmps.2019.02.004

and partial contacts by imposing a boundary condition (Persson et al., 2002). Recently, this so-called Persson theory was applied to study adhesion problems; related work is presented in Persson and Scaraggi (2014) and Wang and Müser (2017). However, this theory cannot predict contact-patch-size distribution effects (Müser et al., 2017), and both asperity models and Persson theory are unable to describe the distribution of surface separation.

On the contrary, numerical contact analyses, which take the real surface topography into consideration, are effective approaches for predicting both the real contact area and the surface separation. There are several subtypes of numerical methods including the boundary element method (BEM) (Hu et al., 1999; Stanley and Kato, 1997), semi-analytical method (Chen et al., 2016; Wang et al., 2010; Li and Berger, 2003; Pohrt and Li, 2014; Carbone and Putignano, 2013), and finite element method (FEM) (Hyun et al., 2004; Pei et al., 2005; Wriggers and Reinelt, 2010; Zhang et al., 2017; Sahoo and Ghosh, 2007; Sarosh et al., 2011; Shi and Zou, 2018). The BEM method is based on the Green function and is efficient for solving linear-elastic contact problems. The semi-analytical method and FEM should be used for elastoplastic contact problems.

Extensive experimental research (Woo and Thomas, 1980) has also been reported. For example, previous studies have measured thermal resistance (Boeschoten and Held, 1957; Sridhar and Yovanovich, 2012), electric resistance (Bhushan, 1985), and the ultrasonic reflection coefficient (Nagy, 1992; Dwyer-Joyce et al., 2001) to evaluate the real contact area between rough surfaces; however, the presence of oxide films and air gaps reduced the accuracy of the results. Optical experiments using surface profilometers (Visscher et al., 1993; Visscher and Struik, 1994; Visscher et al., 1994; Hendriks and Visscher, 1995) or self-designed equipment (Benabdallah and Lapierre, 1990; Bennett et al., 2017; Rohde et al., 2017) have also been conducted to measure the real contact area or the separation between rough surfaces. However, optical methods require at least one surface of the contact pair to be transparent, which is not applicable in most engineering situations.

Experimental research in the field of contact mechanics is relatively less developed than analytical and numerical work, largely because the materials of rough surfaces of engineering interest are usually non-transparent and not accessible for direct visual observation, making it challenging to observe the contact behaviors between non-transparent rough surfaces. Thus, the direct experimental verification of analytical and numerical research of contact problems is challenging (Vakis et al., 2018). In this study, the real contact area and three-dimensional surface separation between non-transparent rough surfaces were experimentally measured using X-ray computed tomography (CT) technology. Contact pairs made of aluminum (Al) and polycarbonate (PC) were measured. In addition, finite element models were constructed to simulate the contact behaviors of the same contact pairs. The results obtained from the finite element analyses and the experiments were compared. The simulation results were in good agreement with the experimental observations when the material properties of the rough surfaces were consistent.

2. Sample preparation

Each contact pair consisted of two faces that were the respective end faces of two cylinders. The cylindrical samples (Fig. 1) were 3 mm in diameter and 10 mm in height. Other details of the cylindrical samples are given in Table 1. The cylinders for each contact pair were numbered $x-1$ and $x-2$, where x is the number of the contact pair. Contact pairs 1 and 3 consisted of a flat surface (samples 1-1 and 3-1) and an anisotropic rough surface (samples 1-2 and 3-2). The flat surfaces of samples 1-1 and 3-1 were manufactured by turning while the rough surfaces of samples 1-2 and 3-2, which had several parallel textures, were manufactured by knurling and milling, respectively. Contact pair 2 consisted of two isotropic rough surfaces (samples 2-1 and 2-2) manufactured by wire electrical discharge machining (WEDM). Contact pairs 1 and 2 were fabricated from Al and contact pair 3 was made from PC. A three-dimensional (3D) surface profilometer was used to

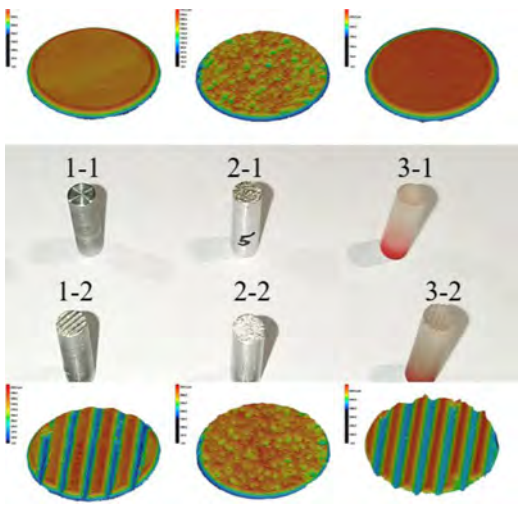

Fig. 1. Experimental contact pairs.

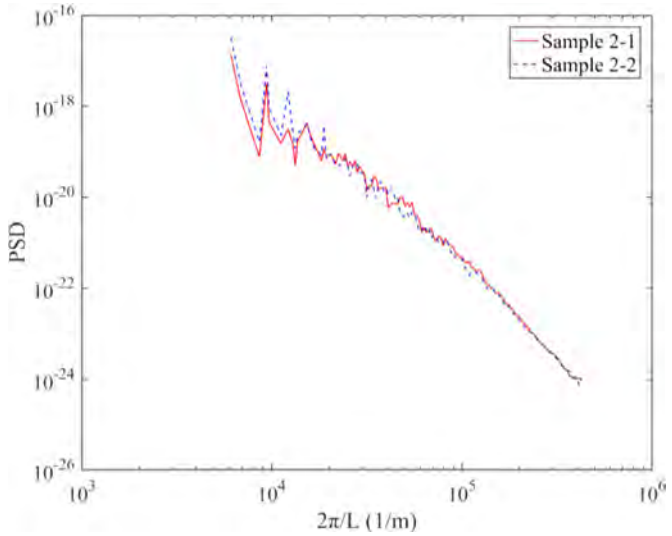

Fig. 2. Power spectral density (PSD) of samples 2-1 and 2-2.

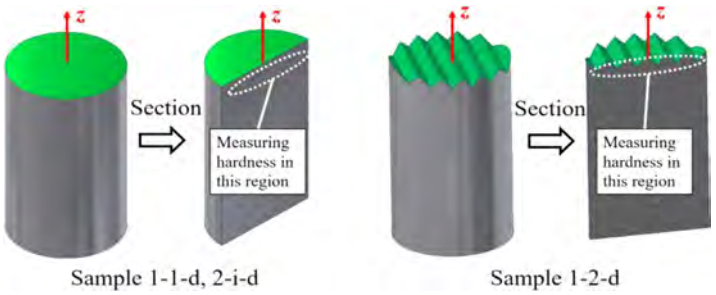

Fig. 3. Schematic diagrams of the sample sectioning.

Table 1
Sample details.

Contact pair	Material[a]	Sample	Type of surface	Processing method[b]	Roughness (μm)
1	Al	1-1	Flat	Turning	3
		1-2	Rough and anisotropic	Knurling	43
2	Al	2-1	Rough and isotropic	WEDM	20
		2-2	Rough and isotropic	WEDM	22
3	PC	3-1	Flat	Turning	3
		3-2	Rough and anisotropic	Milling	60

[a] Aluminum (Al) or polycarbonate (PC).
[b] Wire electrical discharge machining (WEDM).

measure the surface topographies of these contact pairs (Fig. 1). The roughness of the rough surfaces (samples 1-2, 2-1, 2-2 and 3-2) was ca. Ra 20–60 μm. The roughness of the flat surfaces (samples 1-1 and 3-1) was only ca. Ra 3 μm. Furthermore, the power spectral density (Fig. 2) showed that the isotropic rough surfaces of contact pair 2 were approximately fractal.

3. Yield strength measurement

The yield strength near metal contact surfaces can be affected by machining processes. Thus, the real yield strength near each metal contact surface (i.e., the contact surfaces of contact pairs 1 and 2) should be measured for finite element analyses. The yield strength and the Vickers hardness have an approximately linear relationship according to Eq. (1) (Cahoon et al., 1971; Tabor, 1951):

$$\sigma_y = 10 \times H/3 \tag{1}$$

where σ_y (MPa) is the yield strength and H (kg/mm^2) is the Vickers hardness. Thus, after measuring the Vickers hardness near the contact surfaces, the yield strength could be calculated. Each cylindrical sample of contact pairs 1 and 2 (i.e.,

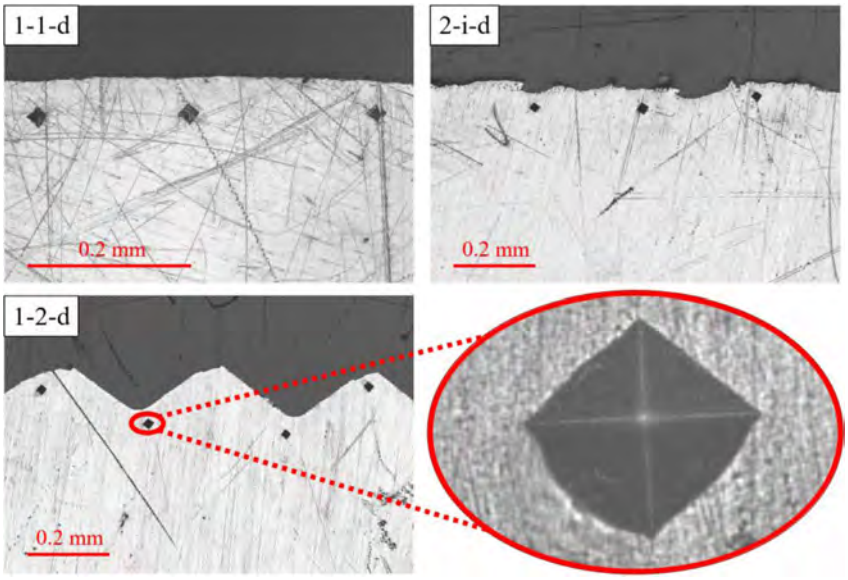

Fig. 4. Measurement of the Vickers hardness near the contact surfaces.

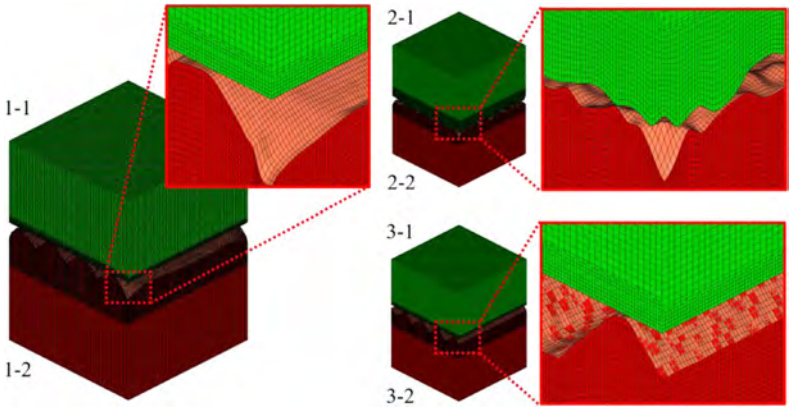

Fig. 5. Finite element models of the three contact pairs.

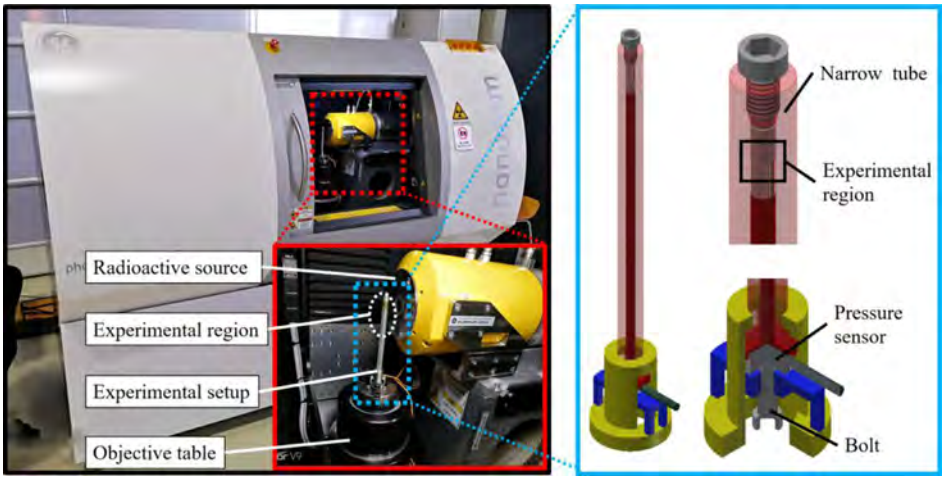

Fig. 6. Experimental equipment and jig.

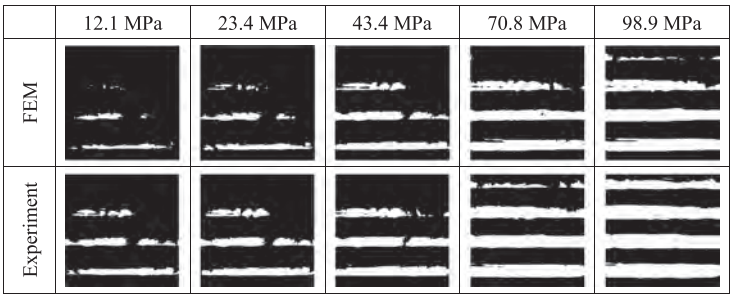

(a) Contact pair 1

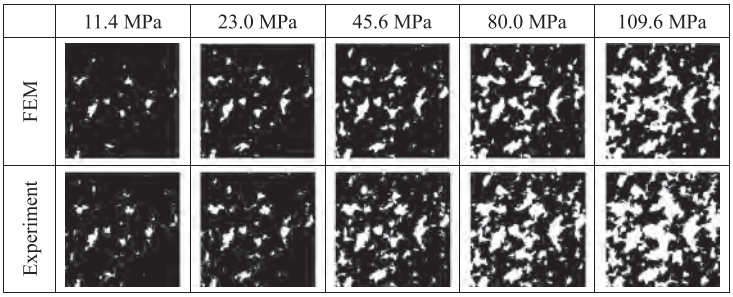

(b) Contact pair 2

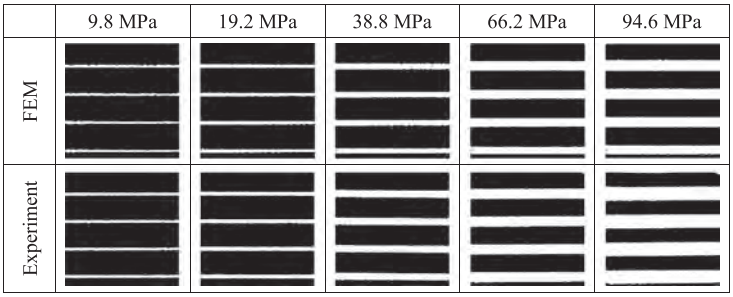

(c) Contact pair 3

Fig. 7. Comparison of the real contact status obtained from the finite element model simulations and the experiments.

Table 2
Vickers hardness of the aluminum surfaces.

Sample		Hardness (kg/mm2)				Yield strength (MPa)
		Point 1	Point 2	Point 3	Average	
1-1-d		28.8	28.6	29.4	28.9	96.3
1-2-d	Peak	32.0	31.4	–	31.7	105.7
	Valley	36.1	37.0	–	36.6	122.0
2-i-d		30.7	32.3	29.9	31.0	103.3

samples 1-1, 1-2, 2-1, and 2-2) had a duplicate that was manufactured by the same process. The duplicate cylindrical samples were numbered as 1-1-d (duplicate of 1-1), 1-2-d (duplicate of 1-2) and 2-i-d (duplicate of 2-1 and 2-2). Cylindrical samples 2-1 and 2-2 were manufactured by the same process; thus, they shared a common duplicate sample. The duplicate cylindrical samples were used for the Vickers hardness measurement because this is a destructive technique. For the measurement, the cylinders were sectioned (Fig. 3) and the hardness was measured near the contact surfaces. Samples 1-1-d and 2-i-d had flat or isotropic surfaces, so they were simply sectioned along the z direction. However, sample 1-2-d had an anisotropic rough surface, so it was sectioned along the z direction and perpendicularly to the texture. The measured points of each sample were close to the surfaces, about 50 to 70 μm below (Fig. 4); the hardness and the yield strength values are given in Table 2. The hardness clearly varied with the manufacturing process. In addition, the hardness was consistent at the various measured points for samples 1-1-d and 2-i-d. However, the hardness for sample 1-2-d, which was measured on a peak of the rough surface, was lower than that measured at a valley of the rough surface. This phenomenon demonstrates that the knurling process affects the yield strength. However, it is very difficult to include this hardness inconsistency in

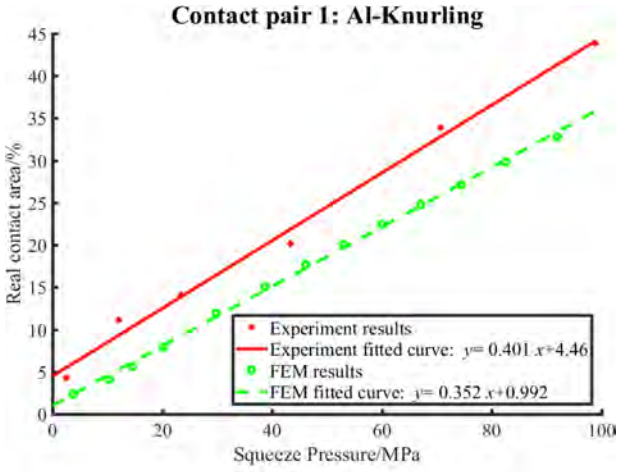

(a) Contact pair 1

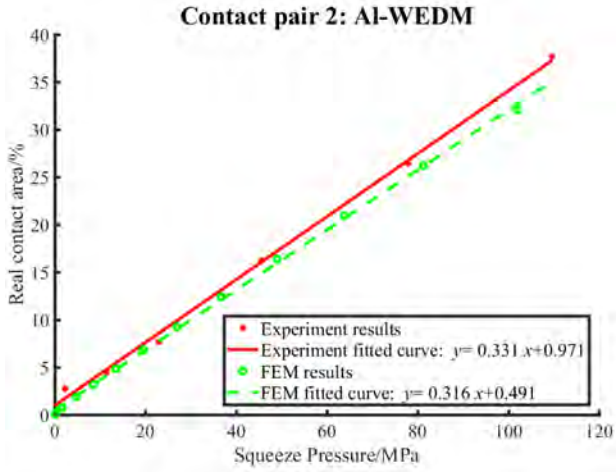

(b) Contact pair 2

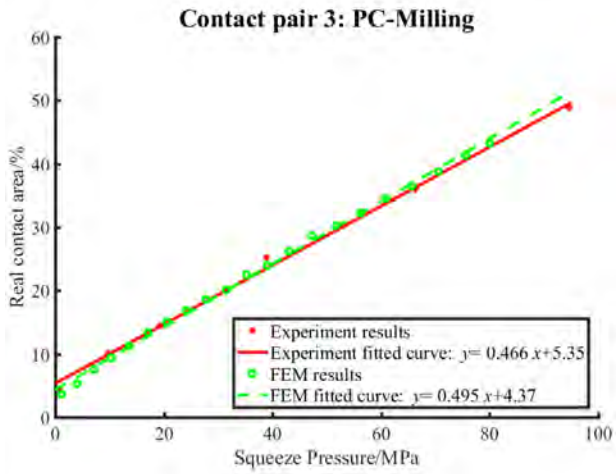

(c) Contact pair 3

Fig. 8. Relationship between the real contact area and the squeeze load.

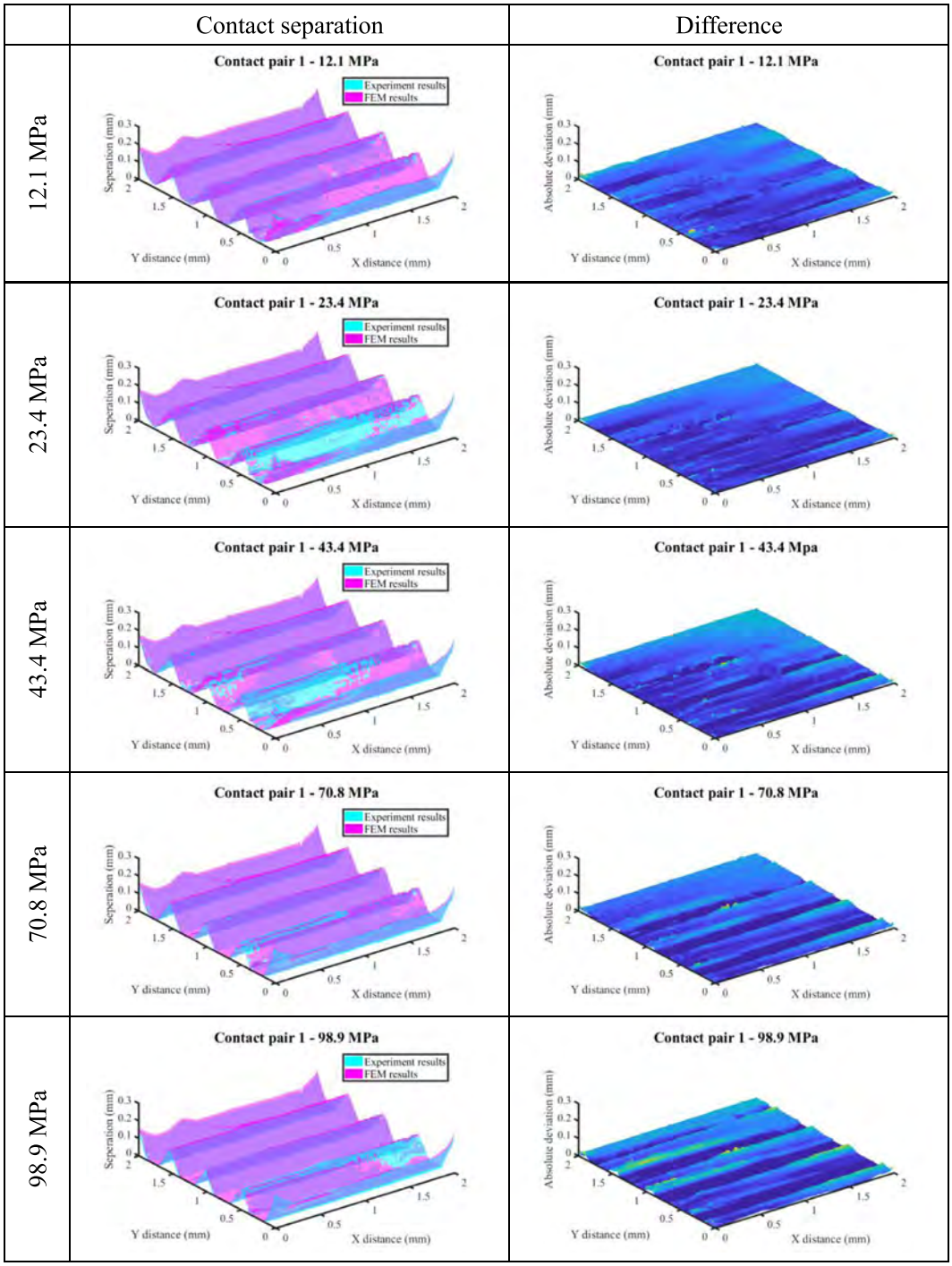

(a) Contact pair 1

Fig. 9. Comparison of the contact separations obtained from the finite element model simulations and the experiments. (The entire contact zones are shown.).

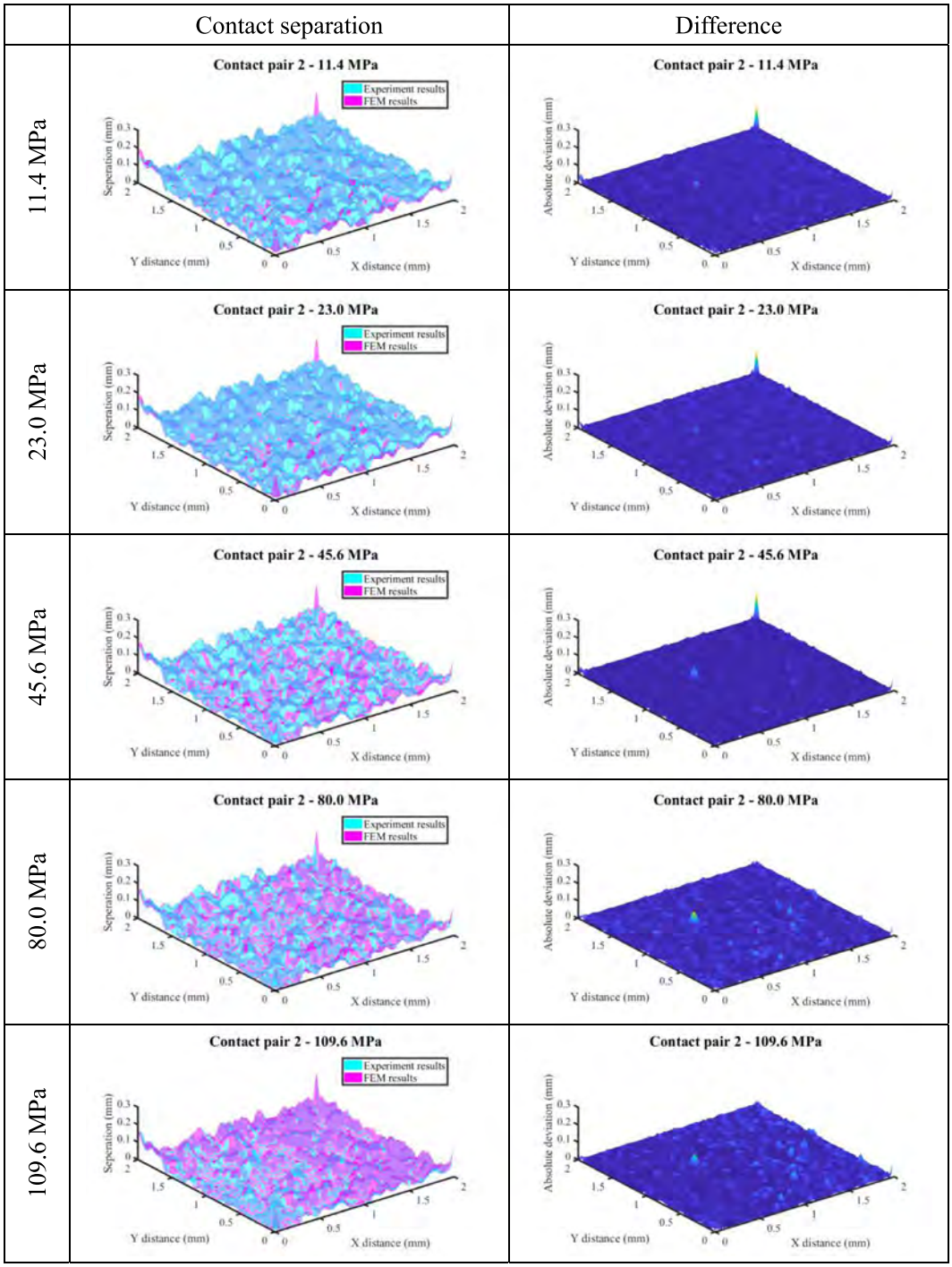

(b) Contact pair 2

Fig. 9. Continued

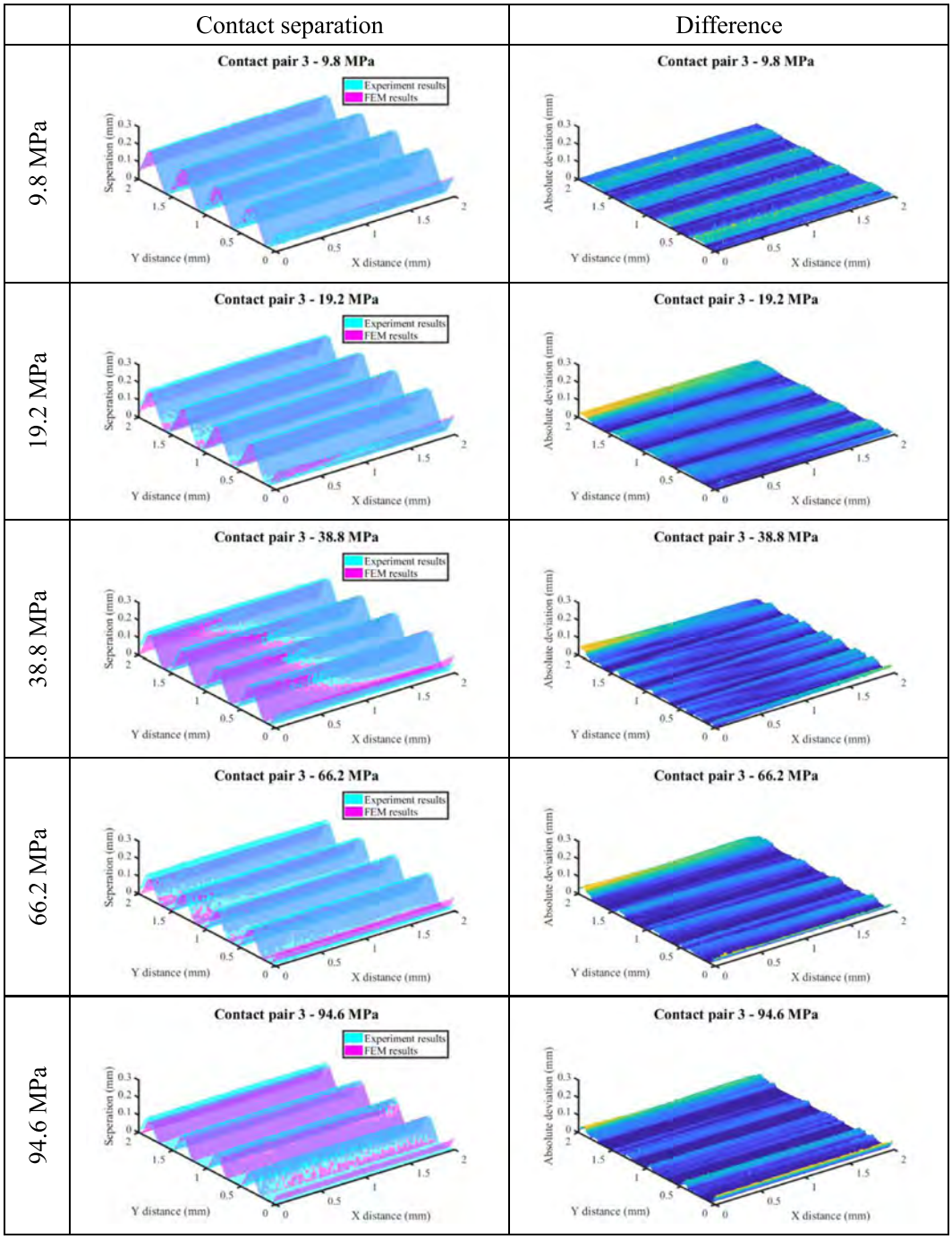

(c) Contact pair 3

Fig. 9. Continued

Table 3
Material properties of the samples.

Sample	Material[a]	Young's modulus (MPa)	Poisson's ratio	Yield strength (MPa)	Tangent modulus (MPa)
1-1	Al	62,000	0.3	96.3	169
1-2				105.7	
2-1				103.3	
2-2					
3-1	PC	1009	0.39	76.0	124
3-2					

[a] Aluminum (Al) or polycarbonate (PC).

FEM simulations. As the surface deformation occurs initially and primarily on the peaks of a rough surface, the yield strength calculated on the basis of the hardness measured on the peaks of sample 1-2-d was used in the following FEM simulations.

4. Finite element modeling

Based on the measured topographies of the rough surfaces, 3D finite element contact models were developed using commercial software. The material properties of Al and PC were defined using a bilinear isotropic model (Table 3). Specifically, the yield strength of samples 1-1, 1-2, 2-1, and 2-2 was obtained from the measurement described in Section 3. Fig. 5 illustrates the two parts of the models, for which each part had dimensions $2 \times 2 \times 1\,mm^3$. The 2×2 mm^2 square contact surfaces were extracted from the centers of the end faces of the cylinders. The bodies of the models were meshed by 3D solid elements (SOLID 45) that were defined by eight nodes. The upper surfaces were defined as the target surfaces, which were meshed with TARGE 170 elements, and the lower surfaces were defined as the contact surfaces, which were meshed with CONTA 173 elements. The zone near the contact surfaces was meshed with the finest elements, and the size of the elements gradually increased with increasing distance from the contact surfaces (Fig. 5). In the finite element models, the fixed constraint was applied on the bottom, and symmetry constraints were applied on the surrounding surfaces. The displacement load was applied on the top. All analyses used a single load step with 100–200 sub-steps. The friction coefficient was set to 0.15. An augmented Lagrangian method was applied, and the preconditioned conjugate gradient solver was used to accelerate the rate of convergence. After a grid refinement study, meshes containing a total of 2,340,000–2,540,000 elements were adopted. In these meshes, the 2×2 mm^2 contact surfaces were meshed by 200×200 grids.

5. Experimental procedure

Fig. 6 shows how X-ray CT technology (Phoenix nanoCT®) was used in this research to measure the real contact area and surface separation between contact pairs. The highest resolution of this system was 0.2 μm. An experimental jig was designed to apply the load and maintain the squeeze pressure on the contact pairs. The samples were confined in a narrow tube; the squeeze load was applied by a bolt and measured using a sensor. The experimental setup was assembled on the objective table of the CT system (Fig. 6). Restricted by the size and density of the contact pairs and the setup, the resolution under the conditions in this experiment was 2 μm. Six squeeze loads, F^*, (5, 50, 100, 200, 350 and 500 N) were gradually applied to the contact pairs, and the real contact area and surface separation between the non-transparent rough surfaces were observed experimentally. The contact behaviors of the 2×2 mm^2 square from the centers of the contact surfaces of the contact pairs were extracted to compare with the finite element results. The squeeze load on the square, denoted as F, was calculated by Eq. (2).

$$\frac{F}{F*}=\frac{A}{A*} \tag{2}$$

where A is the real contact area of the square, A^* is the real contact area of the whole contact pair.

6. Results and discussion

The contact status for each contact pair is shown in Fig. 7, in which the white zone corresponds to the contact zone. The X-ray CT technology enabled direct observation of the normalized real contact area between the non-transparent rough surfaces. The normalized real contact areas obtained by FEM simulations and experiments are in good agreement. Fig. 8 shows the relationship between the normalized real contact area and the squeeze pressure obtained by the experiments and FEM simulations (detailed data of the experimental curves can be found in the Supplementary Material). The real contact area was nearly proportional to the squeeze load in all of the cases. The slopes of the fitted curves in Fig. 8 were calculated. Then the relative difference between the slopes obtained from FEM simulations and those obtained from experiments was obtained (Table 4). Based on the results shown in Figs. 7, 8, and Table 4, we conclude that there were no significant differences between the results of the contact process obtained from the FEM simulations and the experiments. Specifically, the relative difference between the slopes for contact pairs 2 and 3 was less than 4.6% and 6.3%, respectively. However, the

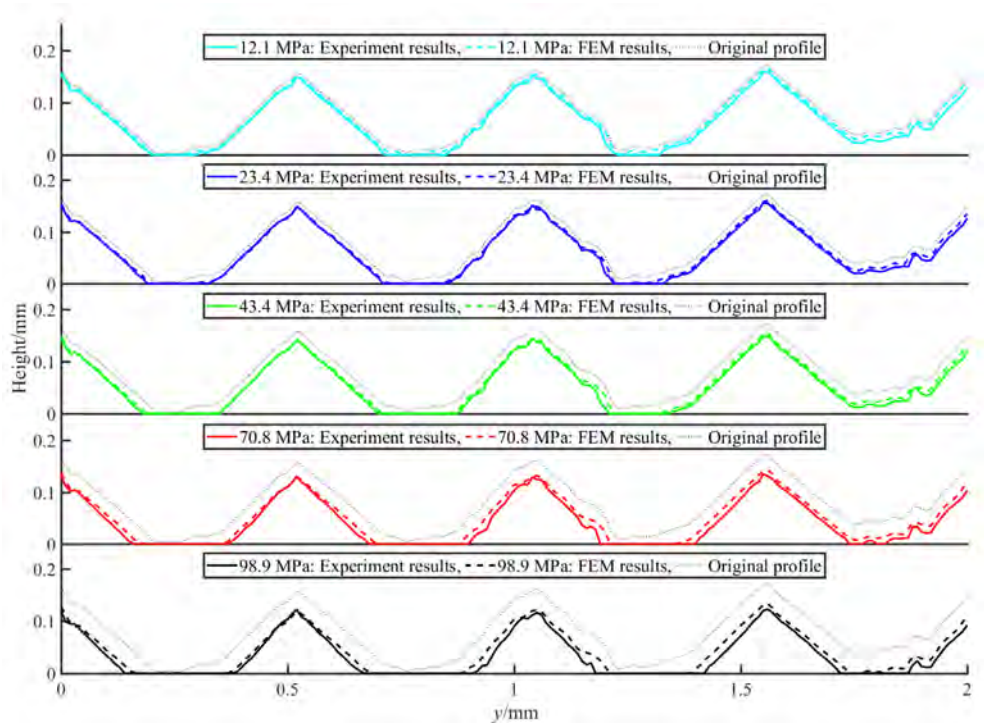

(a) Contact pair 1

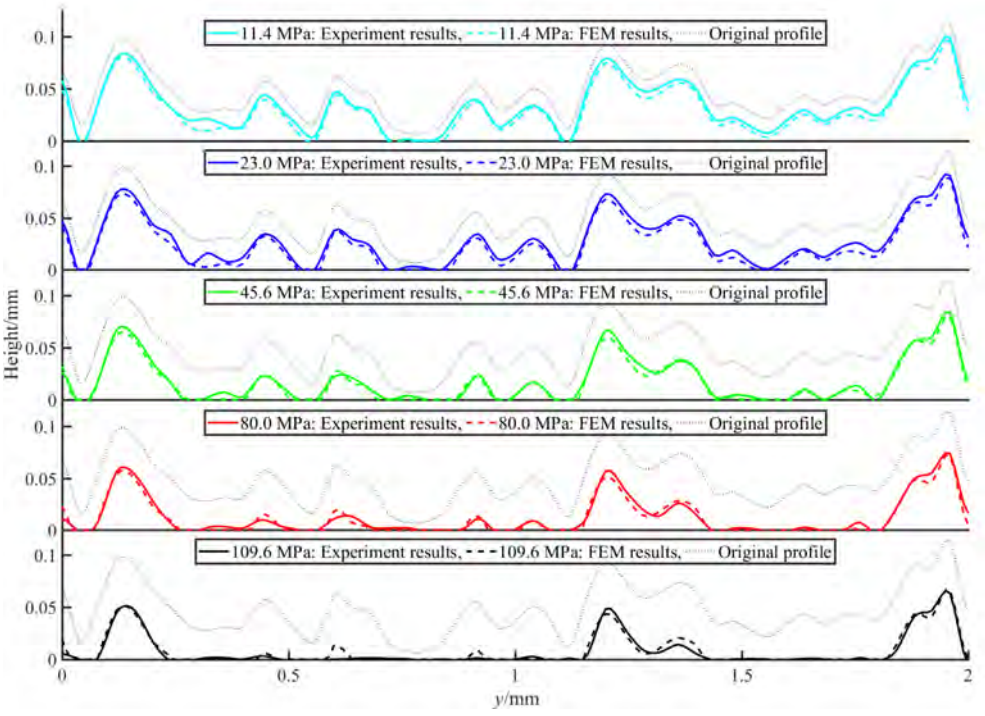

(b) Contact pair 2

Fig. 10. Comparison of the separation profiles obtained from the finite element model simulations and the experiments. (Only profiles are shown.).

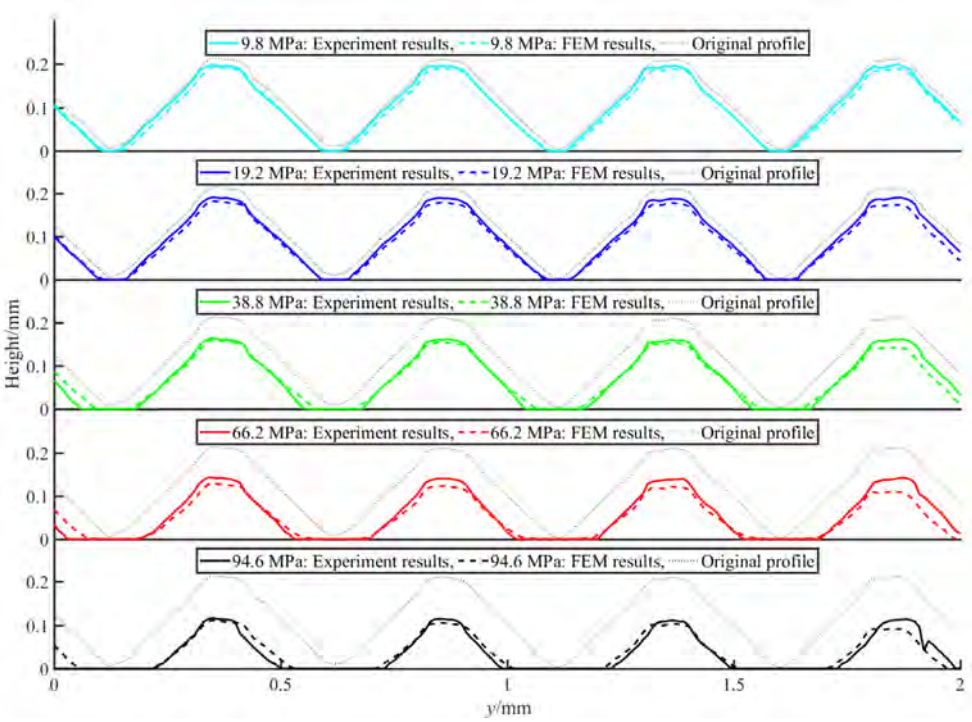

(c) Contact pair 3

Fig. 10. Continued

Table 4
Relative difference between the slopes obtained from finite element analyses and experiments for each contact pair.

	Contact pair 1	Contact pair 2	Contact pair 3
Relative difference	12.22%	4.53%	6.23%

Table 5
Average values of the relative difference between the contact separations obtained from the FEM simulations and the experiments.

Contact pair 1		Contact pair 2		Contact pair 3	
Pressure (MPa)	Relative difference	Pressure (MPa)	Relative difference	Pressure (MPa)	Relative difference
12.1	7.67%	11.4	5.64%	9.8	4.45%
23.4	4.28%	23.0	5.75%	19.2	7.89%
43.4	5.32%	45.6	1.95%	38.8	3.52%
70.8	9.04%	80.0	0.66%	66.2	5.19%
98.9	9.35%	109.6	2.97%	94.6	1.19%

difference between the FEM simulations and the experimental results was quite large for contact pair 1, most likely due to the inconsistency of the yield strength near the contact surface of the sample 1-2, as discussed in Section 3.

As contact pair 2 consists of randomly isotropic rough surfaces (instead of wavy surfaces), the proportionality coefficient between the normalized pressure and the contact area for contact pair 2, denoted as κ, was calculated by Eq. (3).

$$\kappa = \frac{A/A_0}{\sigma_0/\left(E^*\sqrt{\langle\nabla h^2\rangle}\right)} \tag{3}$$

where A/A_0 is the normalized real contact area, σ_0 (MPa) is the average squeeze pressure (calculated based on $\sigma_0 = F/A_0$), $\langle\nabla h^2\rangle$ is the average square slope of the equivalent rough surface (separation between two rough surfaces while the squeeze pressure is 0 MPa) and E^* (MPa) is the equivalent elastic modulus ($E^* = E_1E_2/((1-\nu_1{}^2)E_2 + (1-\nu_2{}^2)E_1)$). The values of κ calculated from the experiment and the elastic-plastic finite element contact simulation are 117.9 and 112.6, respectively. Notably, the results are extremely higher than the value predicted by the multi-asperity model ($\kappa \approx 2.5$) and Persson's theory

($\kappa \approx 1.6$). This is believed to be caused by the plastic deformation of the rough surfaces. To verify this, an elastic finite element contact simulation was conducted based on the same surface topography. Limited by the convergence of the elastic finite element contact model, the calculated highest real contact area was up to around 8%, and the value of κ under this condition was around 2.54.

X-ray CT technology can also directly observe the surface separation between non-transparent rough surfaces. The surface separations obtained from the FEM simulations and the experiments are shown and compared in Figs. 9 and 10 (detailed data of the experimental surface separation can be found in the Supplementary Material). Specifically, Fig. 9 shows the results for the entire contact zone, whereas Fig. 10 shows the results for three randomly selected profiles. Figs. 9 and 10 show the similarity of the surface separations obtained from the FEM simulations and the experiments. The relative difference between the surface separations obtained from these two methods was also calculated. The average values for each case and at each contact pressure are given in Table 5. The relative difference fluctuates with increasing squeeze pressure. However, the relative difference for all scenarios was less than 10%. In addition, the relative difference was greater for contact pair 1 than for contact pairs 2 and 3 due to yield strength inconsistency.

7. Conclusions

An experimental method based on X-ray CT technology was used to measure the real contact area and surface separation between non-transparent rough surfaces at a resolution of 2 μm. Two contact pairs of Al samples and one contact pair of PC samples were manufactured and observed. The 3D contact, specifically, the real contact area and the surface separation, were directly observed. The experimental results were compared to FEM simulations. The simulation results were in good agreement with the experimental observations when the material properties of the rough surfaces were consistent. However, the machining processes may have caused the inconsistency of material properties, such as yield strength, that was observed near the contact surfaces. Ignoring such inconsistencies could significantly increase the error of the results derived from numerical contact analyses.

Acknowledgments

The authors wish to thank Professor J. R. Barber of University of Michigan for his help during the course of this work.

Funding

The Science Challenge Project (Grant no. TZ2018007), the National Natural Science Foundation of China (Grant nos. 51605030 and 51675050), the International Graduate Exchange Program of Beijing Institute of Technology.

Supplementary material

Supplementary material associated with this article can be found, in the online version, at doi:10.1016/j.jmps.2019.02.004.

References

Afferrante, L., Carbone, G., G, D., 2012. Interacting and coalescing Hertzian asperities: a new multiasperity contact model. Wear 278–279 (5), 28–33.
Benabdallah, S.M., Lapierre, J., 1990. A new device for measuring the real area of contact of polymeric material by the perturbation of total internal reflection. J. Mater. Sci. 25 (8), 3497–3500.
Bennett, A.I., Harris, K.L., Schulze, K.D., et al., 2017. Contact measurements of randomly rough surfaces. Tribol. Lett. 65 (4), 134.
Bhushan, Bharat, 1985. The real area of contact in polymeric magnetic media-ii: experimental data and analysis. Tribol. Trans. 28 (2), 181–197.
Boeschoten, F., Held, E.F.M.V.D., 1957. The thermal conductance of contacts between aluminium and other metals. Physica 23 (1), 37–44.
Cahoon, J.R., Broughton, W.H., Kutzak, A.R., 1971. The determination of yield strength from hardness measurements. Metall. Trans. 2 (7), 1979–1983.
Carbone, G., Putignano, C., 2013. A novel methodology to predict sliding and rolling friction of viscoelastic materials: theory and experiments. J. Mech. Phys. Solids 61 (8), 1822–1834.
Chang, W.R., Etsion, I., Bogy, D.B., 1987. An elastic-plastic model for the contact of rough surfaces. J. Tribol. 109 (2), 257–263.
Chen, W.W., Liu, S., Wang, Q.J., 2016. Fast Fourier transform based numerical methods for elasto-plastic contacts of nominally flat surfaces. J. Appl. Mech. 75 (1), 011022.
Ciavarella, M., Delfine, V., Demelio, G., 2006. A “Re-Vitalized” Greenwood and Williamson model of elastic contact between fractal surfaces. J. Mech. Phys. Solids 54 (12), 2569–2591.
Ciavarella, M., Greenwood, J.A., Paggi, M., 2008. Inclusion of “Interaction” in the Greenwood and Williamson contact theory. Wear 265 (5), 729–734.
Dwyer-Joyce, R.S., Drinkwater, B.W., Quinn, A.M., 2001. The use of ultrasound in the investigation of rough surface interfaces. J. Tribol. 123 (1), 8–16.
Greenwood, J.A., Williamson, J.B.P., 1966. Contact of nominally flat surfaces. Proc. R. Soc. Lond. 295 (1442), 300–319.
Hendriks, C.P., Visscher, M., 1995. Accurate real area of contact measurements on polyurethane. J. Tribol. 117 (4), 607–611.
Hertz, H., 1881. On the contact of elastic solids. J. Reine Angew. Math. 92, 156–171.
Hu, Yuan-Zhong, Barber, G., Zhu, Dong, 1999. Numerical analysis for the elastic contact of real rough surfaces. Tribol. Trans. 42 (3), 443–452.
Hyun, S., Pei, L., Molinari, J.F., et al., 2004. Finite-element analysis of contact between elastic self-affine surfaces. Phys. Rev. E Stat. Nonlinear Soft Matter Phys. 70 (2), 026117.
Li, J., Berger, E.J., 2003. A semi-analytical approach to three-dimensional normal contact problems with friction. Comput. Mech. 30 (4), 310–322.
Müser, M.H., Dapp, W.B., Bugnicourt, R., et al., 2017. Meeting the contact-mechanics challenge. Tribol. Lett. 65 (4), 118.
Nagy, P.B., 1992. Ultrasonic classification of imperfect surfaces. J. Nondestruct. Eval. 11 (3), 127–139.
Paggi, M., Ciavarella, M., 2010. The coefficient of proportionality κ between real contact area and load, with new asperity models. Wear 268 (7–8), 1020–1029.
Pei, L., Hyun, S., Molinari, J.F., et al., 2005. Finite element modeling of elasto-plastic contact between rough surfaces. J. Mech. Phys. Solids 53 (11), 2385–2409.

Persson, B.N., 2001. Elastoplastic contact between randomly rough surfaces. Phys. Rev. Lett. 87 (11), 116101.
Persson, B.N., Scaraggi, M., 2014. Theory of adhesion: role of surface roughness. J. Chem. Phys. 141 (12), 124701.
Persson, B.N.J., Bucher, F., Chiaia, B., 2002. Elastic contact between randomly rough surfaces: comparison of theory with numerical results. Phys. Rev. B 65 (18), 184106.
Pohrt, R., Li, Q., 2014. Complete boundary element formulation for normal and tangential contact problems. Phys. Mesomech. 17 (4), 334–340.
Rohde, S.E., Bennett, A.I., Harris, K.L., et al., 2017. Measuring contact mechanics deformations using DIC through a transparent medium. Exp. Mech. 57 (9), 1445–1455.
Sahoo, P., Ghosh, N., 2007. Finite element contact analysis of fractal surfaces. J. Phys. D Appl. Phys. 40 (14), 4245.
Sarosh, B., Danielsson, J., Meijer, J., 2011. Rough surface contact analysis by means of the finite element method and of a new reduced model. Comptes Rendus Mécanique 339 (7), 473–490.
Shi, X., Zou, Y., 2018. A comparative study on equivalent modeling of rough surfaces contact. J. Tribol.
Sridhar, M.R., Yovanovich, M., 2012. Review of elastic and plastic contact conductance models - comparison with experiment. J. Thermophys. Heat Transf. 8 (4), 633–640.
Stanley, H.M., Kato, T., 1997. An FFT-based method for rough surface contact. J. Tribol. 119 (3), 481–485.
Tabor, D., 1951. The hardness of metals. Meas. Tech. 5 (4), 281.
Vakis, A.I., Yastrebov, V.A., Scheibert, J., et al., 2018. Modeling and simulation in tribology across scales: an overview. Tribol. Int.
Visscher, M., Hendriks, C.P., Struik, K.G., 1993. The real area of contact measured on elastomers. Thin Films Tribol. 19, 705–714.
Visscher, M., Hendriks, C.P., Struik, K.G., 1994. Optical profilometry and its application to mechanically inaccessible surfaces part ii: application to elastometer/glass contacts. Precis. Eng. 16 (3), 199–204.
Visscher, M., Struik, K.G., 1994. Optical profilometry and its application to mechanically inaccessible surfaces part i: principles of focus error detection. Precis. Eng. 16 (3), 192–198.
Wang, A., Müser, M.H., 2017. Gauging Persson theory on adhesion. Tribol. Lett. 65 (3), 103.
Wang, D., Xu, C., Wan, Q., 2017. Modeling tangential contact of rough surfaces with elastic- and plastic-deformed asperities. J. Tribol. 139 (5), 051401–051408.
Wang, W.Z., Wang, Z.J., Wang, W.Z., et al., 2010. A numerical elastic-plastic contact model for rough surfaces. Tribol. Trans. 53 (2), 224–238.
Woo, K.L., Thomas, T.R., 1980. Contact of rough surfaces: a review of experimental work. Wear 58 (2), 331–340.
Wriggers, P., Reinelt, J., 2010. Multi-scale approach for frictional contact of elastomers on rough rigid surfaces. Comput. Methods Appl. Mech. Eng. 198 (21), 1996–2008.
Yastrebov, V.A., Anciaux, G., Molinari, J.F., 2015. From infinitesimal to full contact between rough surfaces: evolution of the contact area. Int. J. Solids Struct. 52, 83–102.
Zhang, F., Liu, J., Ding, X., et al., 2017. An approach to calculate leak channels and leak rates between metallic sealing surfaces. J. Tribol. 139 (1).
Zhao, Y., Chang, L., 2001. A model of asperity interactions in elastic-plastic contact of rough surfaces. J. Tribol. 123 (4), 857–864.
Zhao, Y., Maietta, D.M., Chang, L., 2000. An asperity microcontact model incorporating the transition from elastic deformation to fully plastic flow. J. Tribol. 122 (1), 86–93.